ATMOSPHERIC SCIENCE LETTERS
Atmos. Sci. Let. (2015)
Published online in Wiley Online Library
(wileyonlinelibrary.com) **DOI:** 10.1002/asl.581

RMetS
Royal Meteorological Society

Observations of fire-induced turbulence regimes during low-intensity wildland fires in forested environments: implications for smoke dispersion

Warren E. Heilman,[1]* Craig B. Clements,[2] Daisuke Seto,[2] Xindi Bian,[1] Kenneth L. Clark,[3] Nicholas S. Skowronski[4] and John L. Hom[5]

[1]*USDA Forest Service, Northern Research Station, Lansing, MI, USA*
[2]*San Jose State University, San Jose, CA, USA*
[3]*USDA Forest Service, Northern Research Station, New Lisbon, NJ, USA*
[4]*USDA Forest Service, Northern Research Station, Morgantown, WV, USA*
[5]*USDA Forest Service, Northern Research Station, Newtown Square, PA, USA*

**Correspondence to:*
Dr Warren E. Heilman, USDA Forest Service, Northern Research Station, 3101 Technology Blvd., Suite F, Lansing, MI, USA.
E-mail: wheilman@fs.fed.us

Received: 11 December 2014
Revised: 25 March 2015
Accepted: 1 April 2015

Abstract

Low-intensity wildland fires occurring beneath forest canopies can result in particularly adverse local air-quality conditions. Ambient and fire-induced turbulent circulations play a substantial role in the transport and dispersion of smoke during these fire events. Recent *in situ* measurements of fire–atmosphere interactions during low-intensity wildland fires have provided new insight into the structure of fire-induced turbulence regimes and how forest overstory vegetation can affect the horizontal and vertical dispersion of smoke. In this paper, we provide a summary of the key turbulence observations made during two low-intensity wildland fire events that occurred in the New Jersey Pine Barrens.

Keywords: **forest canopy; low-intensity wildland fires; smoke dispersion; turbulence**

1. Introduction

Atmospheric interactions with wildland fires play an important role in fire behavior and the transport and dispersion of wildland fire smoke. The release of heat and moisture from fuel combustion during wildland fires alters the local thermal structure of the lower atmospheric boundary layer and induces turbulent circulations. These turbulent circulations, in combination with the ambient mean flow, can affect fire behavior and the transport and dispersion of smoke (Ward and Hardy, 1991; Clements *et al.*, 2008; Sun *et al.*, 2009). The presence of forest overstory vegetation can further complicate local turbulence regimes through its effect on ambient and fire-induced circulations within the fire environment (Kiefer *et al.*, 2014). A more complete understanding of the local atmospheric turbulence dynamics that occur during wildland fires, many of which occur in forested environments, is needed to build the scientific foundation upon which new and improved predictive tools for fire behavior and local smoke dispersion that more completely account for atmospheric turbulence effects can be developed.

Fortunately, recent advances in atmospheric turbulence monitoring techniques within harsh wildland fire environments have provided new opportunities for measuring and analyzing turbulence regimes in the vicinity of wildland fires, thus advancing our understanding of fire–atmosphere interactions (e.g. Clements *et al.*, 2007; Seto and Clements, 2011; Seto *et al.*, 2013). Building upon these previous wildland fire experiments, this observational study focuses specifically on the effects of forest overstory vegetation on fire-induced atmospheric turbulence regimes during low-intensity wildland fires. Low-intensity fires (maximum vertical turbulent heat fluxes on the order of 150 kW m^2 or less above the flaming region) in forested environments, including prescribed fires used for fuels management, can lead to particularly adverse local air-quality conditions (Achtemeier, 2006) because smoke from these fires may linger for relatively long periods of time within forest vegetation layers and lead to human health and local roadway safety concerns. How smoke from low-intensity fires disperses within forested environments is governed to a large extent by local ambient and fire- and forest overstory-induced turbulent circulations that are present.

In this paper, we present an overview of two prescribed fire experiments conducted in forested environments for the purpose of improving our understanding of the local atmospheric turbulence dynamics that occur

during daytime low-intensity surface fires beneath forest overstory vegetation. Measurements of turbulence regimes before, during, and after fire-front passage (FFP) through *in situ* overstory towers are analyzed and the implications for local smoke dispersion in forested environments are discussed.

2. Experimental design

The two experimental sites for this study were located in the New Jersey Pinelands National Reserve (PNR), an area containing some of the most volatile fire-cycle vegetation in the eastern United States (Hom, 2014). The PNR is surrounded by wildland–urban-interface areas and by some of the densest population centers in the U.S. Parts of the surrounding area have been designated as non-attainment areas for particulate matter ($PM_{2.5}$) and ozone by the U.S. Environmental Protection Agency (EPA) (http://www.epa.gov/oar/oaqps/greenbk/rnstate.html).

The first fire experiment (E1) was conducted on 20 March 2011 in a 107-ha burn block (block center: 39.8726°N, 74.5013°W). Vegetation in the block consisted of Pitch pine (*Pinus rigida* Mill.) and mixed oak (*Quercus* spp.) overstory (∼15–18 m height), with blueberry (*Vaccinium* spp.), huckleberry (*Gaylussacia* spp.), and scrub oaks in the understory. Relative maxima in plant area density occurred near the surface (∼0.13 $m^2\ m^{-3}$) and at about 9 m above the surface within the forest overstory canopy (∼0.08 $m^2\ m^{-3}$). The litter layer on the forest floor consisted of pine needles, shrub foliage, and woody fuels ranging in diameter from 0.6 to 7.6 cm. The second burn experiment (E2) was conducted on 6 March 2012 in a 97-ha burn block (block center: 39.9141°N, 74.6033°W). Vegetation in the E2 burn block consisted of mixed oak and scattered Pitch and Shortleaf (*P. echinata* Mill.) pines in the overstory (∼20–23 m height), and primarily blueberry and huckleberry in the understory. The overall plant area density in the E2 burn block was less than that in the E1 burn block, with values less than 0.01 $m^2\ m^{-3}$ just above the surface and maximum density values ∼0.1 $m^2\ m^{-3}$ at 9 m above the surface. The litter layer in the E2 burn block consisted of oak and shrub foliage, some pine needles, and 0.6 to 7.6 cm diameter woody fuels. Both burn blocks were characterized by sandy soils and were relatively flat.

A network of instrumented 3-, 10-, 20-, and 30-m towers and surface monitoring sites was established within and in the vicinity of the E1 and E2 burn blocks (Figure 1). Instrumentation mounted at multiple levels on the towers provided measurements of the three-dimensional wind speed components (U, V, W), temperature (T), relative humidity (RH), net radiation (R_n), atmospheric pressure (p), radiative heat fluxes, and carbon monoxide (CO) and carbon dioxide (CO_2) concentrations. Instrument sampling frequencies were 0.5 Hz on the 3-m towers and 10 Hz on the 10-, 20-, and 30-m towers, respectively. The high-frequency (10 Hz) component wind-speed measurements, carried out only on the 10-, 20-, and 30-m towers within the burn blocks and on the 10-m control towers outside the burn blocks (see Figure 1), were accomplished via sonic anemometers oriented with their horizontal axes aligned in the east–west and north–south (true north) directions. The same meteorological monitoring strategy (i.e. instrumentation, monitoring levels, sampling frequency) was used for the E1 and E2 experiments.

Using drip torches, the New Jersey Forest Fire Service (NJFFS) initiated surface backing fires along the western and eastern perimeters of the E1 and E2 burn blocks, respectively, in accordance with the observed ambient wind directions. Initial ignitions occurred at 1355 UTC (E1: 0955 EDT) and 1430 UTC (E2: 0930 EST) near the southwestern (E1) and southeastern (E2) portions of the burn blocks and continued along the western (E1) and eastern (E2) burn block perimeters. Ambient near-surface temperatures and relative humidity values ranged from ∼2 to 10 °C and ∼30 to 70% during the E1 experiment and from ∼1 to 8 °C and ∼15 to 36% during the E2 experiment. Under light northeasterly to southeasterly ambient winds (<2.5 m s^{-1}) during the E1 experiment, the E1 fire line generally spread northeastward (spread rate ≈ 1.50 m min^{-1}) through the burn block until reaching the northeastern portion of the burn block around 2100 EDT (∼11-h burn experiment). For the E2 experiment, subsequent fire-line ignitions along north–south oriented plow lines spaced ∼200 m apart in the interior of the burn block following the initial fire-line ignition produced a more complicated burn pattern, with multiple fire lines generally spreading westward (spread rate ≈ 0.33 m min^{-1}) through the burn block against light (<3 m s^{-1}) northwesterly to southwesterly ambient winds. Active burning for the E2 experiment was completed by 1800 EST (∼8.5-h burn experiment). Burning was generally confined to surface fuels, and fire-line widths were ∼1–2 m for both experiments. The amount of time required for the E1 and E2 fire lines to pass through each tower location was ∼1.3 and 3 min, respectively, although the effects of the fire lines on atmospheric conditions at the towers lasted much longer (∼1 h).

Data collected during the experiments were subjected to a despiking and filtering routine to remove erroneous data and data values exceeding 6 standard deviations from running 1-h means. Sonic anemometer data were tilt-corrected (Wilczak *et al.*, 2001) to minimize vertical wind speed errors associated with sonic anemometers not mounted exactly level on the network towers.

The despiked and tilt-corrected 10 Hz sonic anemometer wind speed (U, V, W) and temperature (T) data were divided into 1-h block averaging periods over which mean velocities and temperatures ($\overline{U}$, $\overline{V}$, $\overline{W}$, $\overline{T}$) were computed, with perturbation velocities ($u' = U - \overline{U}$, $v' = V - \overline{V}$, $w' = W - \overline{W}$) and temperatures ($t' = T - \overline{T}$) then computed at each 0.1 s. One-hour block averaging periods were adopted for this study based on the recommendation of Sun *et al.* (2006) for eddy flux measurements over forests. 'Fire

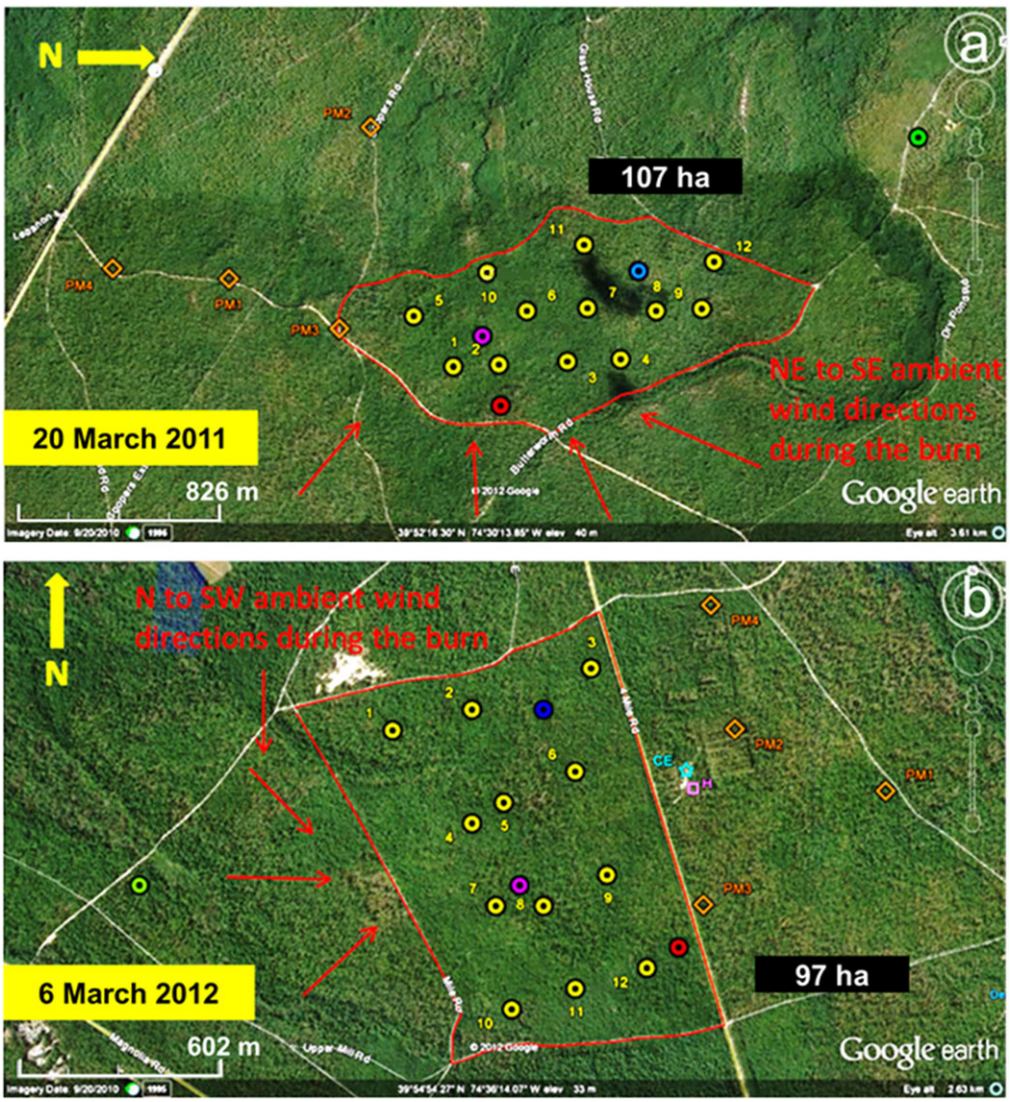

Figure 1. Locations of towers and surface monitoring stations within and in the vicinity of the burn blocks (outlined in red) for the (a) E1 and (b) E2 prescribed fire experiments conducted on 20 March 2011 and 6 March 2012, respectively in the New Jersey Pine Barrens; 3-m towers: numbered yellow circles; 10-m tower: blue circle; 20-m tower: purple circle; 30-m tower: red circle; 10-m control tower: green circle; $PM_{2.5}$ monitors: brown diamonds; ceilometer: blue star; remote helicopter: pink square; SODAR: orange square.

periods' during which FFP occurred at the tower locations were delineated for each tower, with the duration of the periods determined by subjective analysis of the temperature time series obtained from the tower sonic anemometer and thermocouple measurements. Following the methodology of Seto *et al.* (2013), perturbation velocities and temperatures during 'fire periods' were computed by subtracting the mean velocities and temperatures associated with the 1-h period prior to the onset of the 'fire period' from the measured 10 Hz 'fire period' velocities and temperatures. Although one can certainly compute a mean velocity and temperature associated with the fire-induced circulations and heating during the 'fire periods' and then compute corresponding velocity and temperature perturbations from those means, the Seto *et al.* (2013) methodology was adopted so that the computed perturbation velocities and temperatures during the 'fire periods' could provide a better representation of the true fire-induced turbulence and departures from the ambient state that were present. The computed perturbation velocities and temperatures formed the basis for spatial, temporal, and spectral analyses of the turbulence regimes that were present during the experiments.

A complete description of the two fire experiments carried out in this study, including a listing of the instrumentation, measurement strategies, and data analysis techniques, can be found in Heilman *et al.* (2013).

3. Results and discussion

For the analyses of turbulence regimes in the vicinity of the spreading fire lines through the E1 and E2 burn blocks, we focused on observations at the 20-m towers

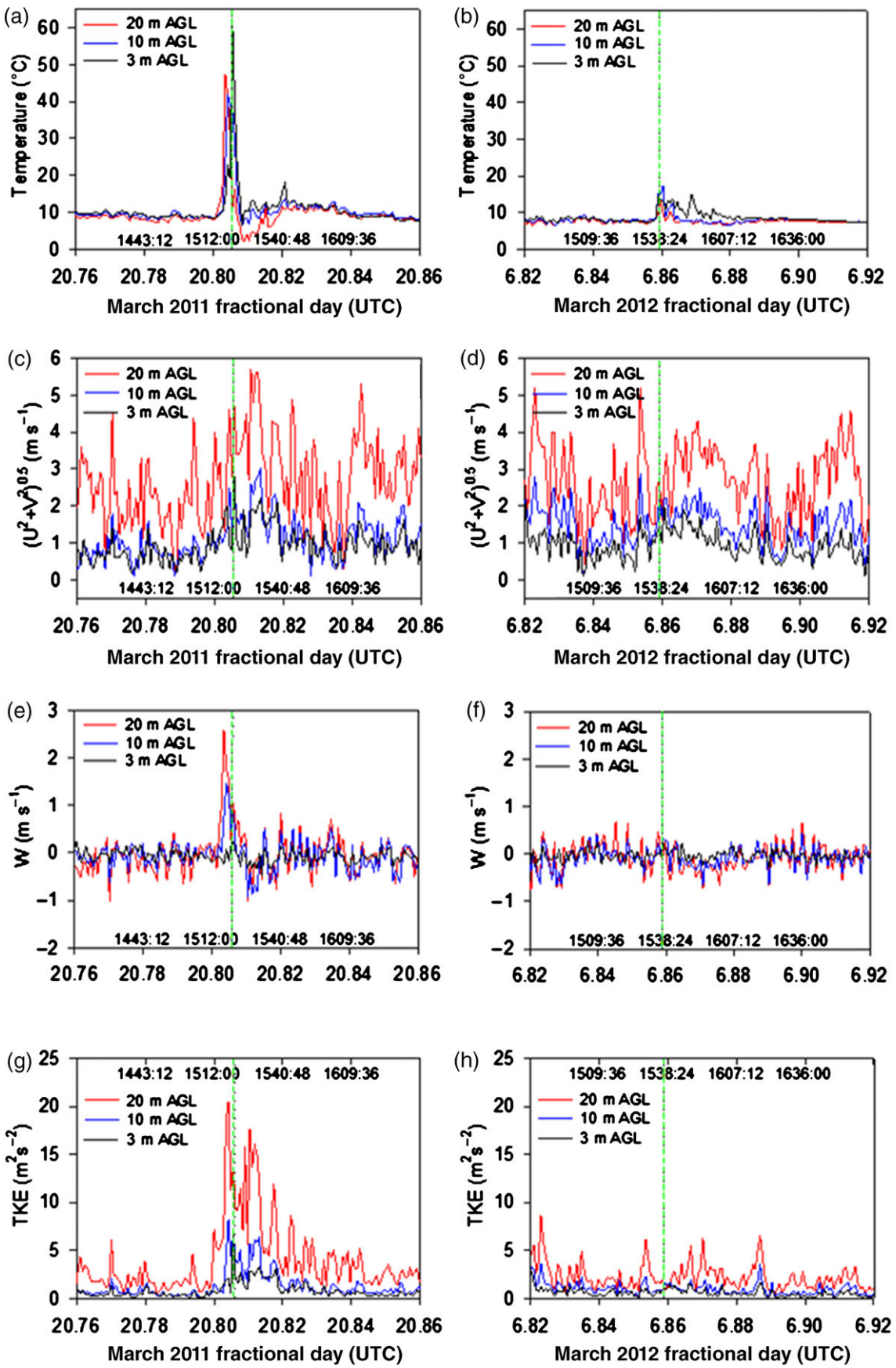

Figure 2. Observed 1-min averaged (a, b) thermocouple temperatures (°C), (c, d) horizontal $[(U^2 + V^2)^{0.5}]$ wind speeds (m s^{-1}), (e, f) vertical (W) wind speeds (m s^{-1}), and (g, h) turbulent kinetic energy (TKE) (m^2 s^{-2}) at three levels on the 20 m towers before, during, and after the E1 (left column) and E2 (right column) fire lines passed the towers. Vertical dashed lines indicate times of fire-front passage (E1: 1520 EDT; E2: 1537 EST). Time stamps (hhmm:ss) in EDT (left column) and EST (right column) are shown above the lower axes or below the upper axes.

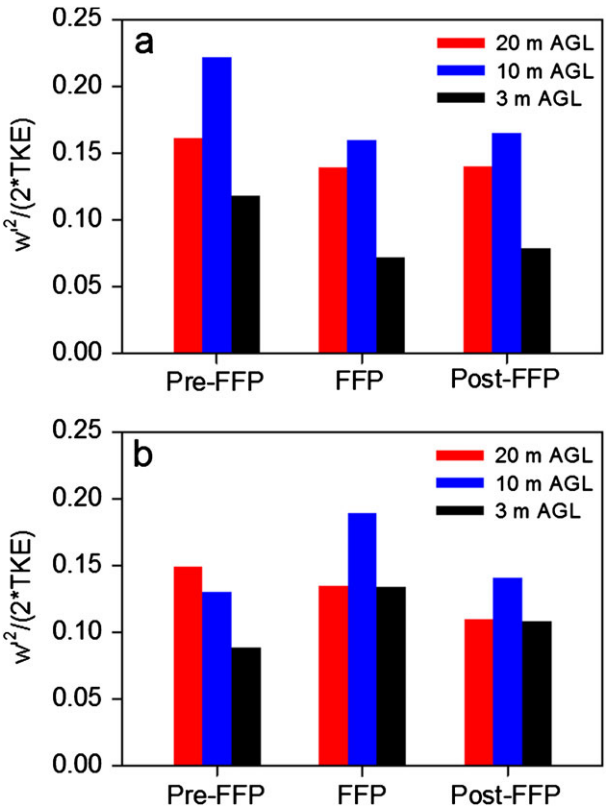

Figure 3. Observed turbulence anisotropy, as quantified by average values of $\overline{w'^2}$/(2*TKE), during the pre-FFP (E1: 1435–1505 EDT; E2: 1452–1522 EST), FFP (E1: 1505–1535 EDT; E2: 1522–1552 EST), and post-FFP (E1: 1535–1605 EDT; E2: 1552–1622 EST) periods at three levels on the 20 m towers located in the interior of the (a) E1 and (b) E2 burn blocks.

primarily because of the availability of sonic anemometer and temperature data both within and near the top of the overstory vegetation layer from those towers. The 20-m towers were also located well-within the boundary of the burn blocks, where observed fire-line spread was less variable and where FFP occurred during daytime conditions for both experiments.

The effects of the fire lines on thermal (T) and kinematic (U, V, W) fields at the 20-m tower locations are shown in Figure 2. Temperature time series (1-min averages) before, during, and after FFP for the E1 and E2 experiments (Figure. 2(a) and (b)) indicate the E1 fire line had a more pronounced local impact on the thermal regime than the E2 fire line. The different temperature responses are consistent with the different maximum vertical turbulent heat fluxes (1-min averages) observed at 3 m AGL above the E1 and E2 fire lines (E1: 23.0 kW m^{-2}; E2: 3.2 kW m^{-2}). Fire-intensity differences were due in part to differences in pre-fire surface fuel loadings (E1: 1.478 ± 0.388 kg m^{-2}; E2: 1.104 ± 0.246 kg m^{-2}) (mean $\pm$ 1 SD), differences in average surface fuel moisture contents (E1: 21.9 ± 9.8%; E2: 49.5 ± 19.6%), and differences in fuel type and arrangement (Heilman *et al.,* 2013). Note that maximum instantaneous (10 Hz) thermocouple temperatures above the E1 and E2 fire lines reached 145.6 and 28.9 °C, respectively.

Consistent with the observed thermal regime variations, local circulation responses to the E1 and E2 fire lines at the 20-m tower locations (Figure 2(c)–(f)) indicate the E1 fire line had a more pronounced local impact on the horizontal $[(U^2 + V^2)^{0.5}]$ and vertical (W) wind speeds than the E2 fire line. FFP through the E1 20 m tower location produced a southeasterly to southwesterly horizontal wind-direction shift and relatively strong updrafts/downdrafts (Figure 2(e)), particularly at 10 and 20 m AGL. FFP through the E2 20-m tower location had a minimal impact on the speed of the ambient horizontal westerly to southwesterly winds (Figure 2(d)) and the speed of the updrafts/downdrafts above the fire line (Figure 2(f)).

The different intensity E1 and E2 fires also generated different turbulence regimes within and near the top of the forest vegetation layers inside the burn blocks (Figure 2(g)–(h)). Turbulence at the 20-m tower locations, quantified by turbulent kinetic energy (TKE) per unit mass (equal to one-half of the sum of the 1-min averaged horizontal and vertical velocity variances ($\overline{u'^2}$, $\overline{v'^2}$, $\overline{w'^2}$) computed from the sonic anemometer component wind-speed measurements), was consistently higher at 20 m (near the canopy top) than at the 10- and 3-m heights. The higher-intensity E1 fire resulted in substantially higher TKE values (Figure 2(g)) within and just above the vegetation layer during and immediately following FFP compared to the E2 fire (Figure 2(h)), with the largest increases occurring at 20 m AGL. At the 20-m level, TKE increased from less than 5 m^2 s^{-2} well before the E1 FFP (1520 EDT) to about 20 m^2 s^{-2} 3 min prior to FFP. TKE values then fluctuated wildly and generally diminished to less than 5 m^2 s^{-2} by ~1610 EDT. At the 10- and 3-m levels, TKE values reached maxima of ~8 m^2 s^{-2} (1517 EDT) and ~7 m^2 s^{-2} (1520 EDT), respectively, and then diminished to less than 2 m^2 s^{-2} by ~1541 EDT. This fire-induced TKE behavior was absent during the lower-intensity E2 fire (Figure 2(h)).

Turbulent mixing of heat, momentum, moisture, and smoke in a particular direction during fire events depends on the distribution of energy among the horizontal and vertical components of the total TKE field. To assess the relative contributions of these components to the total TKE field, a specific measure of turbulence anisotropy, values of TKE$_w$= $\overline{w'^2}$/(2*TKE) were computed for both experiments. Note that TKE$_w \approx 0.33$ under isotropic conditions, whereas TKE$_w \approx 0.14$ for classical atmospheric surface layers (Panofsky and Dutton, 1984). Average observed levels of turbulence anisotropy as measured by TKE$_w$ 30 min before, 30 min during, and 30 min after FFP at the 20-m tower locations for the E1 and E2 experiments are summarized in Figure 3.

Anisotropic turbulence was prevalent during all periods, with the vertical component of TKE usually comprising less than 22% of the total TKE on average. Furthermore, anisotropy tended to be stronger at the 3-m level than at the near-canopy-top 20-m level and the mid-canopy 10-m level. Mean values

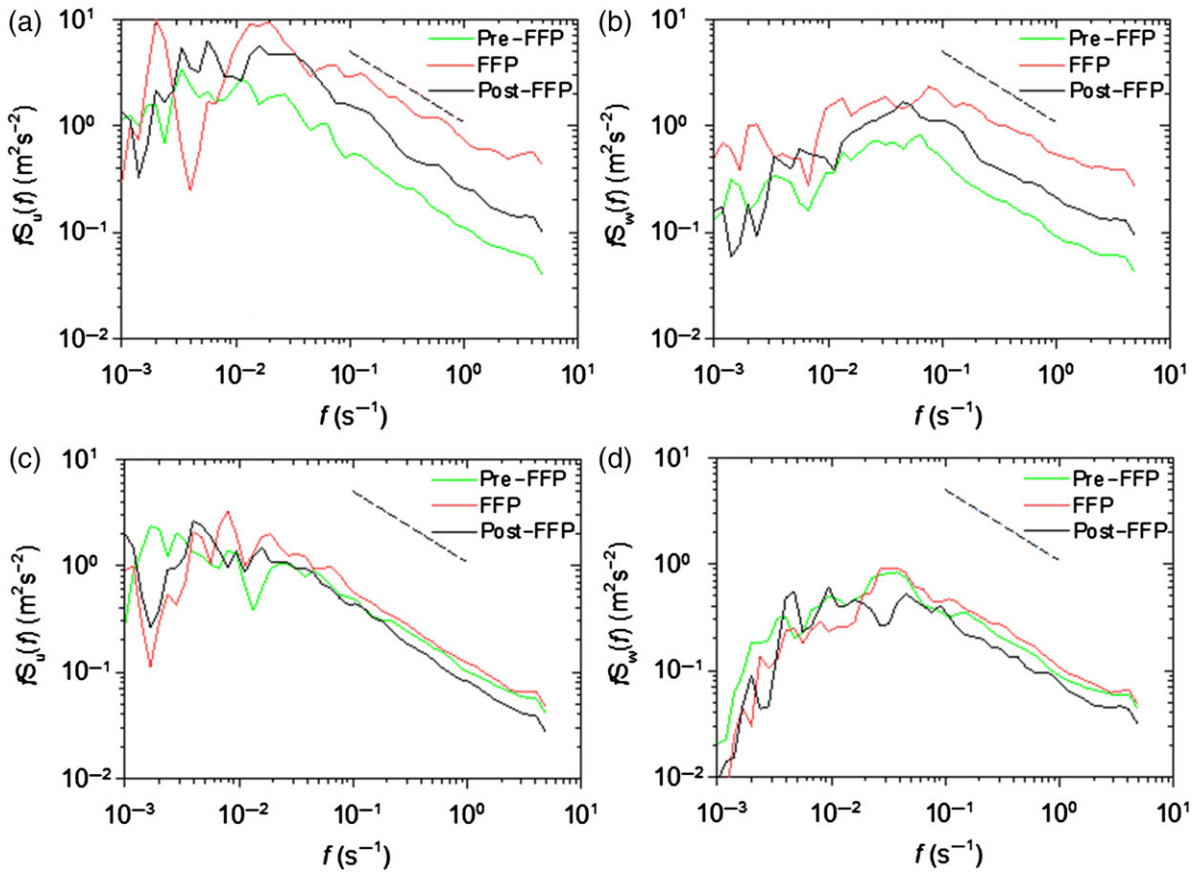

Figure 4. Frequency weighted power spectra (m^2 s^{-2}) at 20 m AGL for the (a, c) horizontal (streamwise) wind velocity [$f\,S_w(f)$] and (b, d) vertical wind velocity [$f\,S_w(f)$] as a function of spectral frequency f (s^{-1}) during the pre-FFP period (E1: 1435–1505 EDT; E2: 1452–1522 EST), the FFP period (E1: 1505–1535 EDT; E2: 1522–1552 EST), and the post-FFP period (E1: 1535–1605 EDT; E2: 1552–1622 EST) for the E1 (top row) and E2 (bottom row) fire experiments. The dashed line represents the theoretical −2/3 slope of spectral power versus frequency curves within the inertial subrange according to Kolmogorov theory.

of TKE$_w$ diminished at all levels from the pre-FFP period to the post-FFP period for the higher-intensity E1 fire (Figure 3(a)). For the lower-intensity E2 fire, mean TKE$_w$ values at the 3- and 10-m levels actually increased during the FFP period (Figure 3(b)). Note that maximum $\overline{w'^2}$ values at each level occurred during the FFP periods for both experiments (E1: 10.72 m^2 s^{-2} at 20 m AGL, 3.71 m^2 s^{-2} at 10 m AGL, 1.25 m^2 s^{-2} at 3 m AGL; E2: 1.12 m^2 s^{-2} at 20 m AGL, 1.25 m^2 s^{-2} at 10 m AGL, 0.45 m^2 s^{-2} at 3 m AGL). This observed behavior in $\overline{w'^2}$ and mean TKE$_w$ values suggests that even though lower-intensity fires in forested environments will probably result in lower overall fire-induced TKE and lower buoyancy-induced vertical velocity perturbations (w') compared to higher-intensity fires, the magnitudes of the vertical velocity perturbations compared to the horizontal velocity perturbations (u' and v') above the fire front may still be large enough such that turbulence fields could actually be less anisotropic than the fields associated with higher-intensity fires.

Using wavelet spectrum analyses (Torrence and Compo, 1998; Seto *et al.,* 2013), anisotropy during the E1 and E2 fires was also assessed in terms of its variation across the different spatial scales (frequencies) of turbulent eddies that contributed to the total TKE fields. The wavelet analyses indicate that the relatively large increases in TKE during FFP for the higher-intensity E1 fire, especially near the canopy top (Figure 2(g)), were associated with energy increases in both the horizontal (streamwise) and vertical velocity perturbations primarily at mid to high frequencies (>10^{-1} s^{-1}) (Figure 4(a) and (b)). Similarly, for the minor changes in TKE during FFP for the lower-intensity E2 fire (Figure 2(h)), slight energy increases in the horizontal (streamwise) and vertical velocity perturbations during FFP were again observed mainly over the mid- to high-frequency portions of the spectrum (Figure 4(c)–(d)). During the E1 post-FFP period, the horizontal and vertical velocity perturbation energies consistently exceeded the energies observed in the pre-FFP period over the mid- to high-frequency portion of the spectrum; the opposite occurred during the lower-intensity E2 fire. Vertical velocity spectra for both fire experiments exhibited peak energy values at the mid-frequency portion of the spectrum (~10^{-1} s^{-1}) before, during, and after FFP, whereas the horizontal (streamwise) spectra exhibited peak energy values at low frequencies (~10^{-3}–10^{-2} s^{-1}). Within the inertial subrange portion of the frequency spectrum, the energy curves exhibited slopes similar to the −2/3 slope suggested by Kolmogorov theory (Kolmogorov, 1941).

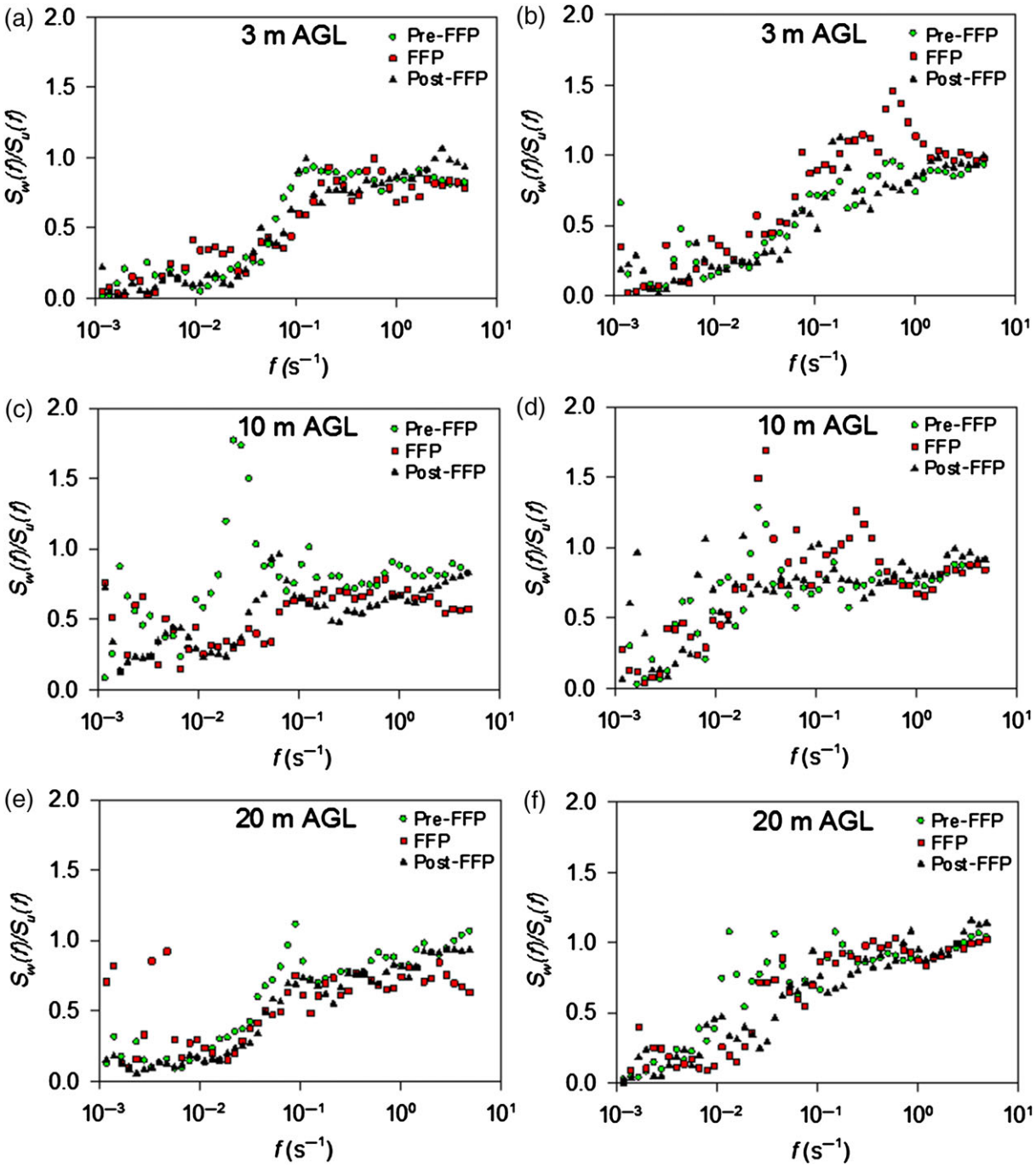

Figure 5. Ratios of the vertical to horizontal (streamwise) power spectra as a function of spectral frequency f (s^{-1}) at (a, b) 3 m, (c, d) 10 m, and (e, f) 20 m AGL during the pre-FFP period (E1: 1435–1505 EDT; E2: 1452–1522 EST), the FFP period (E1: 1505–1535 EDT; E2: 1522–1552 EST), and the post-FFP period (E1: 1535–1605 EDT; E2: 1552–1622 EST) for the E1 (left column) and E2 (right column) fire experiments.

Vertical to horizontal (streamwise) spectra ratios (Figure 5) reveal that low-frequency (large-eddy) turbulent circulations that occurred within and near the top of the vegetation layers during both experiments were more anisotropic than the high-frequency (small-eddy) turbulent circulations, with horizontal (streamwise) turbulence dominating vertical turbulence over most of the low-frequency portion of the spectrum. At higher frequencies, the vertical to horizontal power spectra ratios for both experiments were generally closer to a value of 1 as opposed to the isotropic 4/3 value as predicted by the Kolmogorov (1941) inertial subrange law. This result is consistent with Biltoft (2001), who also provided observational evidence of spectral ratios approaching a value of 1 in the inertial subrange. The dominance of horizontal turbulence over vertical turbulence was prevalent over most of the frequency spectrum regardless of whether a surface fire was present or not (note pre- and post-FFP periods versus FFP periods in Figure 5). As noted in Figure 3, the most anisotropic conditions were generally observed near the surface and canopy top, while turbulence tended to

be a bit less anisotropic at the mid-canopy 10 m level. The power spectra ratios shown in Figure 5 indicate the tendency toward more isotropic conditions at the mid-canopy level occurred primarily over the low- to mid-frequency range of the spectrum ($10^{-3}-10^{-1}$ s^{-1}), which corresponds to eddy sizes greater than ~10–30 m under the observed 1–3 m s^{-1} mean wind speeds within and near the canopy top.

4. Summary and conclusions

Atmospheric turbulence plays an important role in the evolution of smoke plumes during wildland fire events. Turbulence regimes observed during our prescribed fire experiments suggest the presence of forest overstory vegetation during low-intensity surface fires could be an important factor in the local dispersion of smoke from those fires. Depending on actual fire intensity, increases in fire-induced TKE can be much larger at or near the canopy top than at levels just above the surface fire. Under those circumstances, the turbulent mixing or diffusion of smoke as it exits the top of the canopy could be much more substantial than the mixing occurring near the surface and within the vegetation layer. The observations also suggest that turbulence within forest vegetation layers is more anisotropic near the surface and near the canopy top than at mid-canopy levels, with the horizontal component of TKE dominating the vertical component primarily at large eddy sizes (low frequencies). While the presence of a low-intensity surface fire in a forested environment will tend to increase vertical velocity perturbations and the vertical component of TKE due to buoyancy effects, anisotropic turbulence regimes within the forest overstory vegetation layer may still persist. It follows then that horizontal turbulent mixing of smoke from low-intensity surface fires may dominate vertical turbulent mixing processes, particularly near the surface and canopy top.

More research is needed to compare results from this study with turbulence observations during fires of varying intensity in forests characterized by different canopy structure and under different ambient atmospheric conditions. It is through these observational turbulence studies under different environmental conditions that we can develop a better understanding of turbulence regimes that develop during wildland fire events and set the scientific foundation for developing operational air-quality predictive tools that more completely account for forest overstory and fire-intensity impacts on local smoke dispersion.

Acknowledgements

Research support was provided by the U.S. Joint Fire Science Program (Project # 09-1-04-1) and the USDA Forest Service (Research Cost Reimbursable Agreement # 13-CR-11242306-073). We thank the New Jersey Forest Fire Service for managing and conducting the prescribed fires for our experiments. We would also like to thank the anonymous reviewers of this paper for their constructive comments and suggested edits.

References

Achtemeier GL. 2006. Measurements of moisture in smoldering smoke and implications for fog. *International Journal of Wildland Fire* **15**: 517–525.

Biltoft CA. 2001. Some thoughts on local isotropy and the 4/3 lateral to longitudinal velocity spectrum ratio. *Boundary-Layer Meteorology* **100**: 393–404.

Clements CB, Zhong S, Goodrick S, Li J, Potter BE, Bian X, Heilman WE, Charney JJ, Perna R, Jang M, Lee D, Patel M, Street S, Aumann G. 2007. Observing the dynamics of wildland grass fires. *Bulletin of the American Meteorological Society* **88**: 1369–1382.

Clements CB, Zhong S, Bian X, Heilman WE, Byun DW. 2008. First observations of turbulence generated by grass fires. *Journal of Geophysical Research* **113**: D22102, doi: 10.1029/2008JD010014.

Heilman WE, Zhong S, Hom JL, Charney JJ, Kiefer MT, Clark KL, Skowronski N, Bohrer G, Lu W, Liu Y, Kremens R, Bian X, Gallagher M, Patterson M, Nikolic J, Chatziefstratiou T, Stegall C, Forbus K. 2013. Development of modeling tools for predicting smoke dispersion from low-intensity fires. Final Report, U.S. Joint Fire Science Program, Project 09-1-04-1 [Online]. http://www.firescience.gov/projects/09-1-04-1/project/09-1-04-1_final_report.pdf (accessed 25 March 2015).

Hom JL. 2014. Fire research in the New Jersey Pine Barrens. In *Remote Sensing Modeling and Applications to Wildland Fires*, Qu JJ, Sommers W, Yang R, Riebau A, Kafatos M (eds). Springer and Tsinghua University Press: Beijing; 181–191.

Kiefer MT, Heilman WE, Zhong S, Charney JJ, Bian X, Skowronski NS, Hom JL, Clark KL, Patterson M, Gallagher MR. 2014. Multiscale simulation of a prescribed fire event in the New Jersey Pine Barrens using ARPS-CANOPY. *Journal of Applied Meteorology and Climatology* **53**: 793–812.

Kolmogorov AN. 1941. The local structure of turbulence in incompressible viscous fluid for very large Reynolds numbers. *Doklady Akademii Nauk SSSR* **30**: 299–303.

Panofsky HA, Dutton JA. 1984. *Atmospheric Turbulence*. John Wiley and Sons: New York, NY, 397 pp.

Seto D, Clements CB. 2011. Fire whirl evolution observed during a valley wind-sea breeze reversal. *Journal of Combustion* **2011**: 569475, doi: 10.1155/2011/569475.

Seto D, Clements CB, Heilman WE. 2013. Turbulence spectra measured during fire front passage. *Agricultural and Forest Meteorology* **169**: 195–210.

Sun XM, Zhu ZL, Wen XF, Yuan GF, Yu GR. 2006. The impact of averaging period on eddy fluxes observed at ChinaFLUX sites. *Agricultural and Forest Meteorology* **137**: 188–193.

Sun R, Krueger SK, Jenkins MA, Zulauf MA, Charney JJ. 2009. The importance of fire–atmosphere coupling and boundary-layer turbulence to wildfire spread. *International Journal of Wildland Fire* **18**: 50–60.

Torrence C, Compo GP. 1998. A practical guide to wavelet analysis. *Bulletin of the American Meteorological Society* **79**: 61–78.

Ward DE, Hardy CC. 1991. Smoke emissions from wildland fires. *Environment International* **17**: 117–134.

Wilczak JM, Oncley SP, Stage SA. 2001. Sonic anemometer tilt correction algorithms. *Boundary-Layer Meteorology* **99**: 127–150.

